Check for updates

Two-dimensional MXO/MoX$_2$ (M = Hf, Ti and X = S, Se) van der Waals heterostructure: a promising photovoltaic material†

Aman Kassaye Sibhatu, [ID] [ad] Georgies Alene Asres, [ID] [b] Abubeker Yimam[a] and Tamiru Teshome [ID] *[c]

Nanoscale materials with multifunctional properties are necessary for the quick development of high-performance devices for a wide range of applications, hence theoretical research into new two-dimensional (2D) materials is encouraged. 2D materials have a distinct crystalline structure that leads to intriguing occurrences. Stacking diverse two-dimensional (2D) materials has shown to be an efficient way for producing high-performance semiconductor materials. We explored a 2D nanomaterial family, an MXO/MoX$_2$ heterostructure (M = Hf, Ti and X = S, Se), for their various applications using first-principles calculations. We discovered that all of the heterostructure materials utilized are direct band gap semiconductors with band gaps ranging from 1.0 to 2.0 eV, with the exception of hexagonal HfSeO/MoSe$_2$, which has a band gap of 0.525 eV. The influence of strain on the band gap of this HfSeO/MoSe$_2$ material was investigated. In the visible range, we obtained promising optical responses with a high-power conversion efficiency. With fill factors of 0.5, MXO/MoX$_2$ photovoltaic cells showed great PCE of up to 17.8%. The tunable electronic characteristics of these two-dimensional materials would aid in the development of energy conversion devices. According to our findings, the 2D Janus heterostructure of MXO/MoX$_2$ (M = Hf, Ti and X = S, Se) material is an excellent choice for photovoltaic solar cells.

1 Introduction

Materials science and engineering are now more crucial than ever in everyone's lives. Solar power conversion into other kinds of energy, such as electricity (photovoltaic system) is a viable renewable energy generation approach for meeting the world's rising energy demand.[1] Alternative energy sources with no or low greenhouse emissions are promising ways to address environmental and energy issues.[2,3] Advanced materials are essential for energy absorption, conversion, and utilization technologies. Two-dimensional semiconductors are utilized in photocatalysts and photovoltaics, which are currently the focus of study in order to achieve a promising material for sustainable

energy generation due to its innovative features,[4,5] optically distinct and electronic properties.[6] Despite the fact that the researcher's primary focus area is the intensified development of semiconductor materials, which still face multiple significant challenges in producing effective semiconductors, in order to address these challenges, the development of new and more efficient semiconductor materials is required.[4] Today, the basic strategy in advanced materials science and engineering research is to tailor the materials to achieve the desired efficiencies and functionalities.[2] For example, a Si-based photovoltaic cell has material quality and quantity disadvantages.[7] Photovoltaic cells face cost, performance, and operating long lasting challenges.[8] As a result, researchers are working hard to improve the performance of the PCE. Some solar cell research findings in 2D layered van der Waals heterostructures at 2% tensile strain, the PCE of MoSSe/g-GeC is 10.3% (ref. 9) SeIn$_2$Te/C$_2$N and TeIn$_2$Se/C$_2$N vdWHs have PCEs of around 12 and 16%, respectively[10] and for AAII-Se stacking MoS$_2$/MoSSe and MoS$_2$/WSSe a PCE of 12.15% and 9.37%, respectively.[11] It suggests that improving the PCE and other performance factors will take a lot of effort. To address these issues, various 2D materials need to be use with proper Janus and TMDCs that allow for the creation of favorable energy offsets that drive electron–hole separation.[12] The following TMD monolayer materials are significant for the development of photovoltaic cells, such as MoS$_2$ potential for solar cells,[11] MoSe$_2$ fast photodetection.[13] These materials can

[a] Department of Chemical Engineering, School of Chemical and Bio Engineering, Addis Ababa Institute of Technology, Addis Ababa University, Addis Ababa, Ethiopia. E-mail: abubeker.yimam@aau.edu.et; Tel: +251 911950214

[b] Center for Materials Engineering, Addis Ababa Institute of Technology, School of Multi-disciplinary Engineering, Addis Ababa, 1000, Ethiopia

[c] Department of Physics, College of Natural and Social Science, Addis Ababa Science and Technology University, P. O. Box 16417, Addis Ababa, Ethiopia. E-mail: tamiruteshome@gmail.com; Tel: +251 966 253 809

[d] Department of Chemical Engineering, College Biological and Chemical Engineering, Addis Ababa Science and Technology University, P. O. Box 16417, Addis Ababa, Ethiopia

† Electronic supplementary information (ESI) available. See https://doi.org/10.1039/d2ra03204j

bridge the gap owning to their superior optical, electronic, and physical properties, as well as better controllable tuning of physical dimensions. In addition, the layered structure nature of two-dimensional/two-dimensional van der Waals heterostructures have gained a lot of attention recently. They have interesting properties like tunable electronic bandgap, optical absorption, efficient charge separation and transfer, coupling effect, and low quantum confinement[12,14–17] Janus TMDs materials, which differ from traditional 2D materials, have sparked considerable interest. Janus TMDs materials have distinct properties such as asymmetric crystal structure, intrinsic out-of-plane polarization, and piezoelectricity.[18–23] The 2D/2D van der Waals heterostructures coupling is important, it produces a variety of interesting effects[24,25] it is a useful method for combining various properties from 2D different materials[26] to promote PV technology innovation.[27] By stacking the two monolayers together, the MXO/MoX$_2$ heterostructure can be constructed based on this advantage and tunable properties.[28] According to the report, special phenomena will emerge as the two-dimensional materials layer thickness continues to decrease because it is easy to tune and control the functionalities.[29–32] Several 2D materials have been proposed in terms of electronic and optical properties for photovoltaic cells, photodetectors, and photocatalysts.[33–35] Two-dimensional materials have a lot of potential in PV compared to typical photovoltaic solar energy conversion materials.[36] In general, the development of 2D heterostructures results in novel material enhancements.[10] But the heterostructure MXO/MoX$_2$ has yet to be studied. So, in order to investigate the unprecedented unique properties, we proposed hexagonal and distorted heterostructures; such as H-HfSeO/MoSe$_2$, H-HfSO/MoSe$_2$, H-TiSeO/MoSe$_2$, H-TiSO/MoSe$_2$ and T-HfSeO/MoSe$_2$, T-HfSO/MoSe$_2$, T-TiSeO/MoSe$_2$, T-TiSO/MoSe$_2$ stack to investigate the potential of optical properties for PV application.[15,23,37] We investigated the electronic and optical properties of the materials in a systematic manner. Janus (MXO) and TMDs (MoX$_2$) are the general formulas for the crystal structure, where M is a group IV atom (Zr, Ti) and X is a chalcogen (S, Se). Valance electron configuration of hafnium ($4f^{14}$ $5d^2$ $6s^2$), titanium ($3d^2$ $4s^2$), molybdenum ($4d^5$ $5s^1$), sulfur ($3s^2$ $3p^4$), selenium ($3d^{10}$ $4s^2$ $4p^4$), and oxygen ($2s^2$ $2p^4$).

2 Computational methods

Our calculations were carried out using the Vienna *ab initio* simulation package (VASP) based on density functional theory (DFT) with the projector augmented-wave method.[22,38–40] A general gradient approximation of Perdew, Burke, and Ernzerhof (PBE).[32] To account for the PBE functional's underestimated band gap, we used the hybrid density functional Heyd–Scuseria–Ernzerhof (HSE06).[41] Vacuum space was set to 25 Å along the *c*-axis to differentiate the interactions of the adjacent layer. The Brillouin zone was sampled using the Monkhorst–Pack scheme, and a mesh is adopted of $9 \times 9 \times 1$ and $15 \times 15 \times 1$ the wave function expansion of the kinetic energy cutoff set to 520 eV. The convergence threshold criterion is less than 0.01 eV Å^{-1} for ionic relaxation and set for the energy up to 10^{-5} eV.

Optical absorption characteristics were investigated by setting up a *k* grid $15 \times 15 \times 1$. The optical properties calculations for all heterostructures are based on the frequency-dependent dielectric function.[18] The binding energy between the two monolayers is used to calculate the hetero-structure stability, based on the equation which is defined as[42] expressed in eqn (1) below.

$$E_b = E_{MXO/MoX_2} - E_{MXO} - E_{MoX_2} \tag{1}$$

where, E_b is the binding energy, E_{MXO}, E_{MoX_2} and E_{MXO/MoX_2} total energy of the mono-layers: Janus, TMDs and heterostructure, respectively. The optical properties were calculated using the time-dependent (TD) DFT scheme to include electron–hole interactions[43] in the random phase approximation (RPA) approach, which includes local field effects at the Hartree level. Only transitions between bands are considered. For a transitionally invariant system, the Fourier transform of the frequency-dependent symmetric dielectric matrix in the RPA is given by.[44]

$$\varepsilon_{\mathbf{G},\mathbf{G}'}(\mathbf{q}, \omega) = \delta_{\mathbf{G},\mathbf{G}'}(\mathbf{q}, \omega) - \frac{4\pi e^2}{|\mathbf{G} + \mathbf{q}||\mathbf{G}' + \mathbf{q}|}\chi^0_{\mathbf{G},\mathbf{G}'}(\mathbf{q}, \omega) \tag{2}$$

where $\mathbf{G}$ and $\mathbf{G}'$ are reciprocal lattice vectors and $\mathbf{q}$ stands for the Bloch vector of the incident wave. The matrix $\chi^0(\mathbf{q}, \omega)$ is the irreducible polarizability matrix in the case of the independent particle derived by Adler and Wiser[45,46] in the context of the self-consistent field approach. Optical properties of any system are in general calculated with the help of a frequency dependent complex dielectric function $\varepsilon(\omega) = \varepsilon_1(\omega) + i\varepsilon_2(\omega)$. The imaginary part is determined by a summation over empty states using the equation:

$$\varepsilon_2(\omega) = \frac{4\pi^2 e^2}{\Omega} \lim_{q \to 0}\frac{1}{q^2} \sum_{c,v,k} 2\omega_k \delta(E_{ck} - E_{vk} - \omega) \times \langle \mu_{ck} + \boldsymbol{e}_{\alpha q}|\mu_{vk}\rangle$$
$$\times \langle \mu_{ck} + \boldsymbol{e}_{\beta q}|\mu_{vk}\rangle^*$$

where ω, the frequency of electromagnetic (EM) radiation in energy unit is Ω represents the volume of the primitive cell, q is the electron momentum operator, c and v are the conduction band and valence state, respectively, ω_k, is the k point weight E_{ck}, E_{vk} and μ_{ck}, μ_{vk} are the eigenvalues and wave function at the k point, respectively and $\boldsymbol{e}_\alpha$, $\boldsymbol{e}_\beta$ are unit vectors for the three Cartesian direction.

3 Result and discussion

3.1 Structural and energetic stabilities

2D Janus MXO/MoX$_2$ heterostructures (M = Ti, Hf; X = S or Se) are derivatives of their TMD MX$_2$ counterparts (M = Ti, Hf; X = S or Se). MXO monolayers, like MX$_2$, are composed of three atomic layers stacked in the sequence X–M–O, with the crystal structure arranged in two different ways.[16,47] Hexagonal and distorted the ESI Fig. S1† shows a top and side view of the hexagonal and distorted Janus and TMDs monolayer with its heterostructure. To build the most equilibrium configuration of the hexagonal and distorted MXO/MoX$_2$ hetero-structure, individual monolayers are initially investigated. The calculated unit
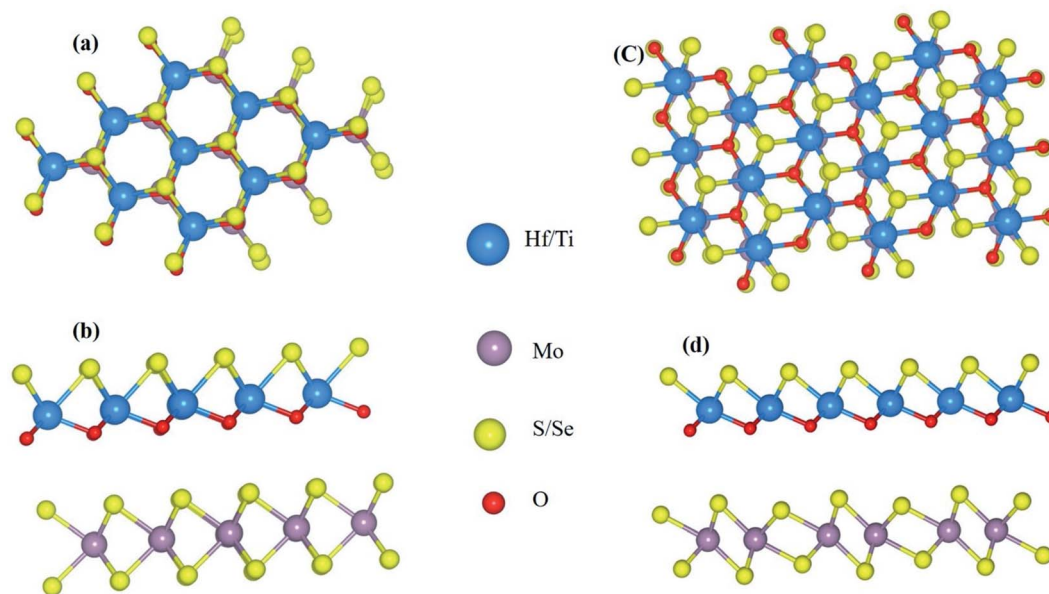
Fig. 1 Diagram geometrical structure (a) top and (b) side views of MXO/MoX$_2$ (M = Ti or Hf; X = S or Se) heterostructure in 2H phase; (c) top and (d) side views of MXO/MoX$_2$ in 2T phase. M (M = Ti or Hf), Mo, X (S or Se), and O are represented by the blue, grey, yellow, and red spheres, respectively.

cell lattice constants and band gap of HfSeO, HfSO, TiSeO, TiSO, MoSe$_2$ and MoS$_2$ are 3.4 Å & 1.3 eV, 3.32 Å & 2.67 eV, 3.15 Å & 1.2 eV, 3.1 Å & 1.6 eV, 3.3 Å & 1.5 eV and 3.2 Å & 1.53 eV respectively, the monolayer's sample band structure and PDOS in the ESI data Fig. S2 and S3,† the obtained results coincide with the earlier findings (Fig. 1).[16,47]

We checked various stacking configurations of the heterostructure to explore the one with the highest stability. Hence, the phase structure of 2D materials governs the physical and chemical properties.[23] By construct the possible stacking configurations for 2H-phase 1 × 1 unit cell stacking AA, A$_1$A, AA$_1$ and for 2T-phase 2 × 2 MXO and MoX$_2$ monolayers were stacked on top of one another to create the distorted MXO/MoX$_2$ heterostructures A$_1$, A$_2$, A$_3$ & A$_4$ stacking. Based on this configuration A$_1$A from the 2H-phase and A$_2$ from 2T the phase has the lowest binding energy which is the more stable one in comparison to the other stacking and selected. The binding energy was found to be negative, indicating that the formation of the MXO/MoX$_2$ heterostructure configurations are energetically favourable.[38,48] The calculated heterostructure binding energy is close to the theoretically predicted value and, in some cases, more stable than the other typical vdW heterostructures listed as; MoS$_2$/WSSe, MoS$_2$/MoSTe, & MoS$_2$/MoSSe is −13, −3 and −9 meV respectively.[11] Experimentally measured binding energies of MoS$_2$/MoSe$_2$ is in between −100 meV to −200 meV (ref. 49) graphene/WSe$_2$ is −55.92 meV,[50] GaN/Bas is −57 meV,[51] graphene/MoS$_2$ is −58.1,[52] Tables S1, S2 and Fig. S4 in the ESI section† illustrate the various stacking binding energy, band gap, and PDOS results. The negative energies indicate the structural stability of the materials. As a result, the most stable configurations of heterostructures are considered in the following discussion.

One of the criteria for classifying a material to form a van der Waals heterostructure is the interlayer distance, better to be in the range of 3–4 Å.[53] The interlayer distance of the van der Waals heterostructure is typical van der Waal equilibrium spacing within the acceptable range, as shown in Table 1. The lattice mismatch is the other important parameter to take into account when considering a material as a van der Waals heterostructure.[54] The two-dimensional monolayer is easily transferred onto a two-dimensional crystal substrate to form a van der Waals heterostructure that allows the combination of lattice mismatched materials.[55] The lattice matching ratio between two individual monolayers is good to be less than 5%.[56,57] The structural match of crystals can be measured using the lattice mismatch, expressed as $\delta = \dfrac{a_n - a_c}{a_n}$ where a_n and a_c are the lattice constants of the optimized Janus and TMDs monolayer respectively.[58] The calculated value of the lattice mismatch of the constructed MXO/MX$_2$ vdW heterostructure is in Table 1

Table 1 The calculated heterostructure lattice mismatch (Δ), interlayer distance (d), binding energy (E$_b$) and bandgap (E$_g$)

Janus/TMDs heterostructures	Δ (%)	d (Å)	E$_b$ (eV)	E$_g$ (eV) PBE	HSE06
H-HfSeO/MoSe$_2$	2.94	3.819	−0.178	1.396	1.655
H-TiSeO/MoSe$_2$	4.54	3.834	−0.234	1.443	2.202
H-HfSO/MoS$_2$	3.61	3.859	−0.093	1.669	2.102
H-TiSO/MoS$_2$	3.11	3.836	−0.139	1.972	2.701
T-HfSeO/MoSe$_2$	4.14	4.005	−0.194	0.525	0.714
T-TiSeO/MoSe$_2$	4.24	4.002	−0.149	1.014	1.303
T-HfSO/MoS$_2$	4.18	3.980	−0.114	1.056	1.205
T-TiSO/MoS$_2$	4.29	3.940	−0.113	1.464	1.824

below indicates suitable calculation results all results are less than 5% which concise with other lattice mismatch of van der Waals heterostructure such as; MoS_2/CdS is 3.92%,[59] SrS/SrSe is 3.91%,[56] GaN/BAs is 4.53%,[57] MoS_2/MoSTe is (5.059%)[11] so that it is possible to form a van der Waal heterostructure. Based on the aforementioned parameters, we determined that the material is a vdW heterostructure.

It is worth noting that the atomic bond lengths d_{M-O} and d_{M-X} are inequitable due to electronegativity and atomic size. For example, $d_{Ti-Se} = 2.7048$ Å which is larger than $d_{Ti-O} = 2.1092$ Å. Regarding the Janus structure the distinction between the top and bottom atoms leads to the charge being more transferred d_{Ti-O} than from d_{Ti-Se}. The calculated heterostructure is shown in Table 1. Bandgap, binding energy, lattice mismatch, and Interlayer distance are all variables to consider.

3.2 Electronic structures

To determine the characteristics of electrons that the individual atom contributions to the chosen hexagonal and distorted structure, the orbital projected density of states (PDOSs) was computed. Fig. 2(a–d) and 3(a–d) depict the heterostructure's 2H and 2T phases, respectively. From the PDOS conduction band maximum is dominated by the 2s orbital of the O atom above the Fermi and is mainly contributed by the 5d orbitals of Hafnium atoms below the Fermi level and also above and below the Fermi level in the 2T-phase heterostructure, 4p and 2s orbitals dominated, respectively. As shown in Fig. 2(a), below

the Fermi level, the 5d orbital of $HfSeO/MoSe_2$ is the main contributor to the valence band, whereas the 4p of Se and 2s oxygen atoms contribute to the conduction band. There is a large shift of the conduction bands towards the Fermi level for $TiSeO/MoSe_2$, as seen in Fig. 2(b), and there is also an overlap between the O (d) orbitals and the Ti (d) orbitals. Fig. 3(d) shows a similar picture for the $TiSO/MoS_2$ system. Due to the electron transfer is crucial for the PDOS's apparent characteristics. Fig. 3(a–d) depicts distorted heterostructure to demonstrate that the MXO contributes not only to the lowest CB but to the highest VB where the highest VB are commonly formed by s-electrons and the bottom-most CB is formed by d-electrons.

The MXO layers gave rise to the VBM and CBM. The PDOS findings suggest that building an MXO and MoX_2 based heterostructure is advantageous for energy-related semiconductor materials. All monolayers of the Janus material are indirect band gap,[16,47] whereas the heterostructure MXO/MoX_2 are all obvious direct band gap semiconductors. The band gap values that were calculated for the heterostructure are listed in Table 1, except for the distorted $HfSeO/MoSe_2$ heterostructure, all the calculated band gap values are in the range of between 1–2 eV, indicating that the values are suitable for photovoltaic applications.[40] For the case of we $HfSeO/MoSe_2$ investigated this material's strain effect on the bandgap shown Fig. S5 and S6 in the ESI.† The Heyd–Scuseria–Ernzerhof hybrid functional (HSE06) is also used to obtain more accurate band gap values. We investigated the power conversion efficiency of the heterostructures below for further analysis.
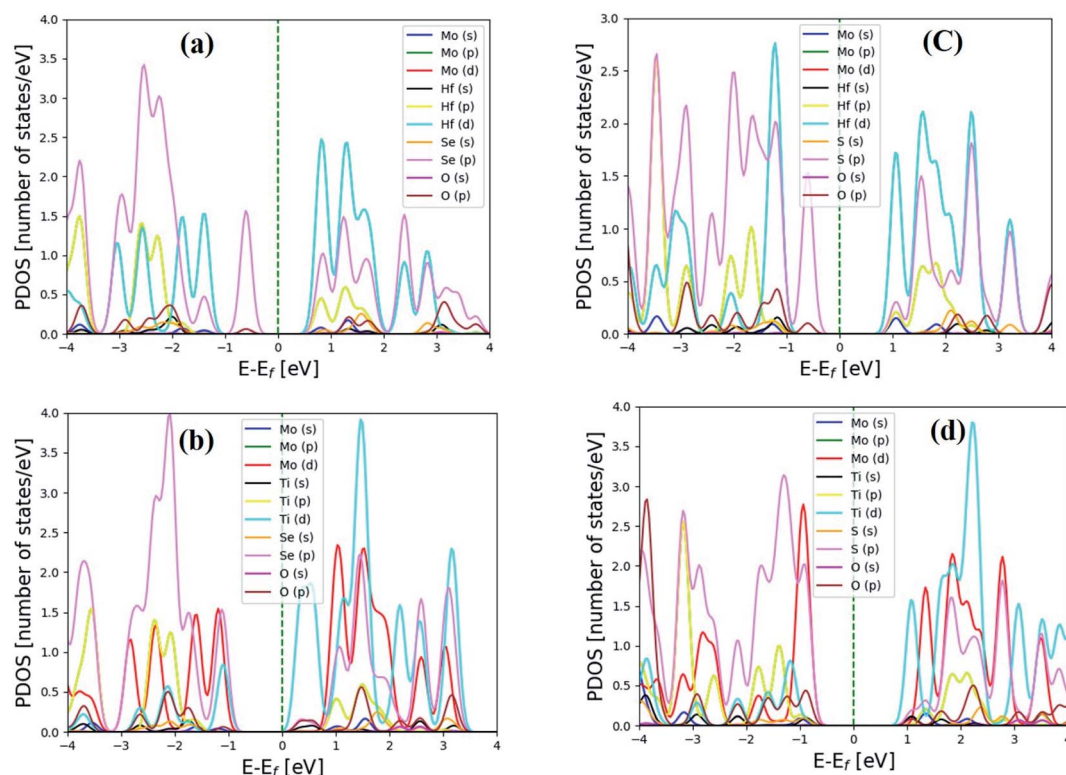

Fig. 2 Electronic projected density of state (PDOS) for 2H heterostructure of (a) $HfSeO/MoSe_2$, (b) $TiSeO/MoSe_2$, (c) $HfSO/MoSe_2$, and (d) $TiSO/MoSe_2$. The Fermi level has been set to a value of zero.
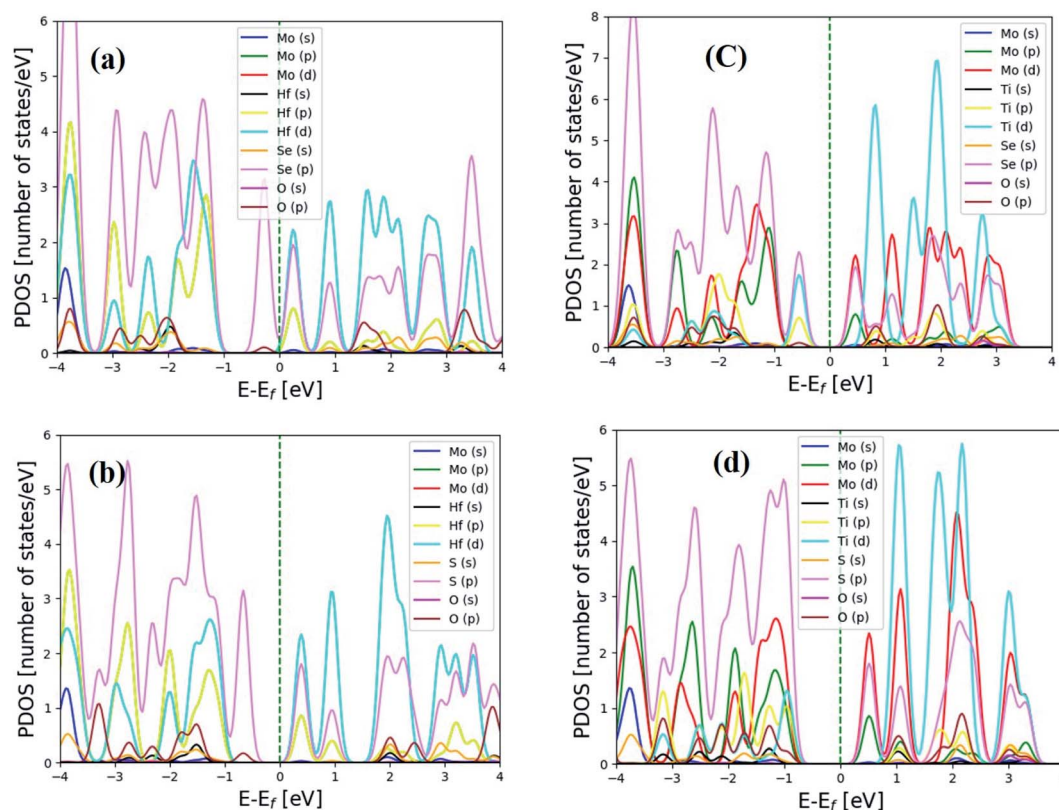
Fig. 3 Electronic projected density of state (PDOS) for 2T-phase (a) HfSeO/MoSe$_2$, (b) HfSO/MoS$_2$, (c) TiSeO/MoSe$_2$, and (d) TiSO/MoS$_2$ heterostructure. The Fermi level has been set to zero.

3.3 Optical properties of the heterostructure

In the optical spectra, one can expect only π to π* and σ to σ* transitions as allowed if the light is polarized parallel to the heterostructure of Janus MXO/MoX$_2$. In contrast, only π to σ* and σ to π* transitions are allowed if the light is polarized perpendicular to the heterostructure. One of the most significant criteria to consider when constructing photovoltaic devices is the optical absorption properties of MXO/MoX$_2$ heterostructures. We were computed and described the frequency dependent imaginary part of the dielectric function $\varepsilon_2(\omega)$ hence it is inextricably linked to the electronic band structure of the material. The complex dielectric function $\varepsilon(\omega) = \varepsilon_1(\omega) + i\varepsilon_2(\omega)$, where $\varepsilon_2(\omega)$ and $\varepsilon_1(\omega)$ are the imaginary and real parts of this dielectric function. The absorption spectrum as shown in Fig. 4(a–d) hexagonal of MXO/MoX$_2$ heterostructures.

We predicted that MXO/MoX$_2$ has absorption peaks in the visible region, with contributions from the O (s) and Hf/Ti (d) orbitals. For the 2T-phase of HfSeO/MoSe$_2$, HfSO/MoS$_2$, TiSeO/MoSe$_2$, and TiSO/MoS$_2$, the notable maximum peaks are 4.4 eV, 3.4 eV, 5.3 eV, and 2.1 eV, respectively. Fig. 5(a–d) shows the dielectric function $\varepsilon_2(\omega)$ of distorted MXO/MoX$_2$ vdWs heterostructures in the visible/UV spectral region of 0–6.2 eV.

As a result, the maximum optical absorption peak for the 2T phase of HfSeO/MoSe$_2$, HfSO/MoS$_2$, TiSeO/MoSe$_2$, and TiSO/MoS$_2$ was seen at 4.2 eV, 3.4 eV, 3.5 eV, and 4.0 eV, respectively. One of the most defining characteristics of 2D semiconductors

is their synergistic relationship with light. The photovoltaic should absorb visible light to maximize energy conversion. The calculated value of the visible light-absorbing semiconductor material. In general, heterostructures have a high dielectric constant, and the dielectric function value at zero energy is critical for photovoltaic applications. Which are very similar to the most promising material in photovoltaic cells.

3.4 Solar photovoltaic cells

van der Waals heterostructures with reduced layer thicknesses are a promising new development technology for ultrathin, small, and light PV solar energy.[60,61] A suitable band gap is required for the stable MXO/MoX$_2$ heterostructure, which is important for photovoltaic cells.[62] We obtained a band-gap range that have a strong absorbance in the visible range. The most commonly used parameter to assess the performance of solar cell in power conversion efficiency (PCE).[63] As a result, the effectiveness of all these heterostructures in photovoltaic applications is assessed based on the PCE value calculated. The efficiency of a solar cell is defined as the ratio of energy output to input energy of the sun.[64] Using[65] method, we computed the power conversion efficiency (PCE) η of the MXO/MoX$_2$ vdW heterostructure. To compute the maximum PCE the most important indicator for describing a photovoltaic device is with the following equation used to calculate the PCE, which is articulated below.
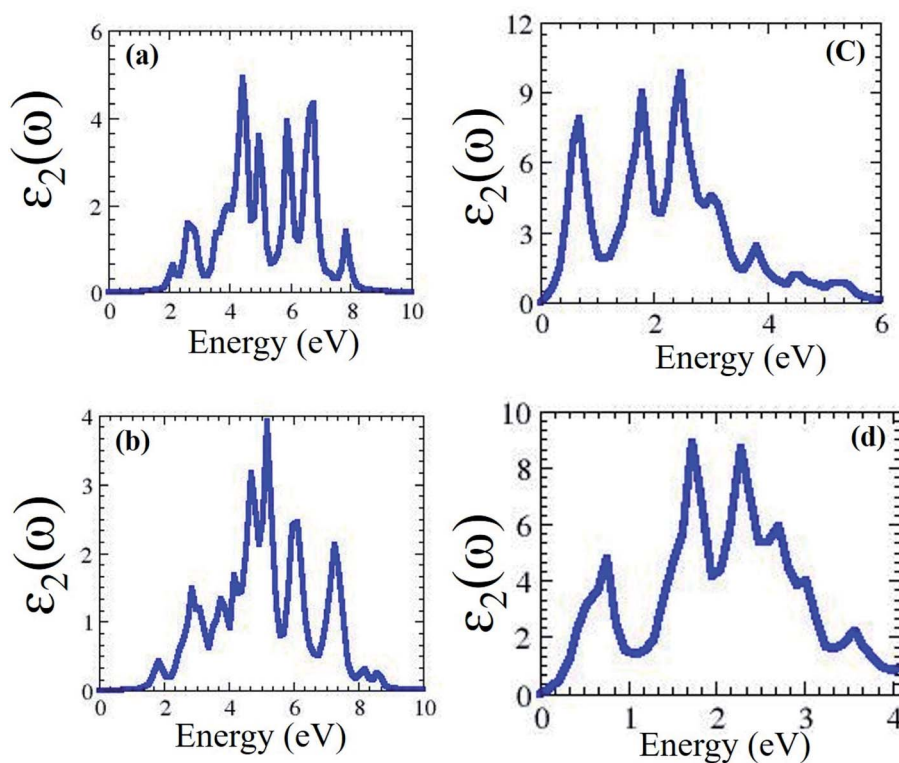
Fig. 4   2H phase optical properties for (a) HfSeO/MoSe$_2$, (b) HfSO/MoS$_2$, (c) TiSeO/MoSe$_2$, and (d) TiSO/MoS$_2$ heterostructure.
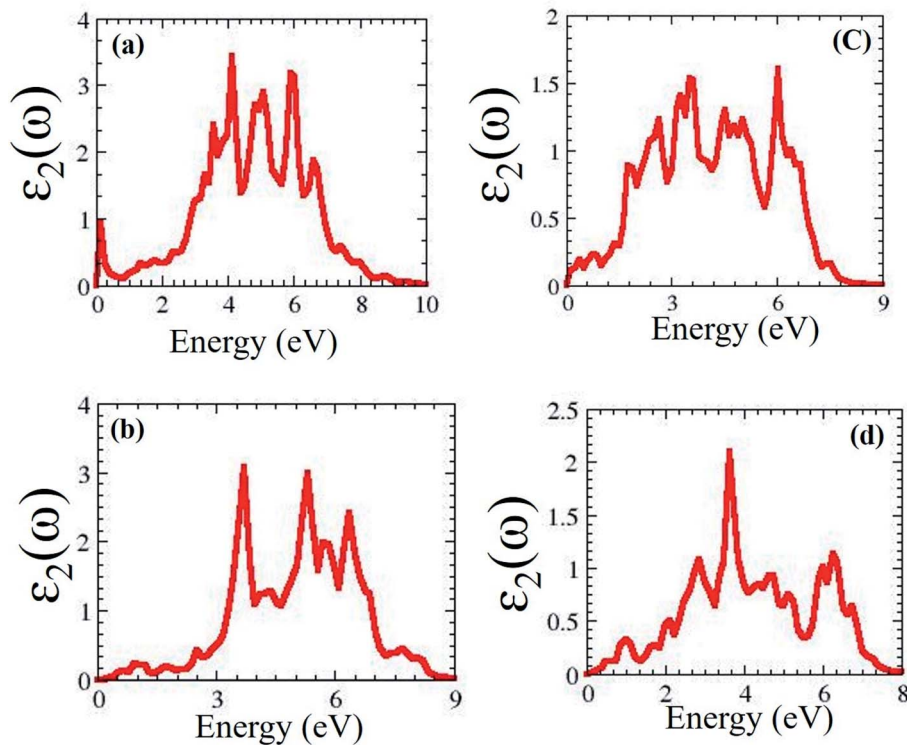

Fig. 5   Optical properties of 2T-phases (a) HfSeO/MoSe$_2$, (b) HfSO/MoSe$_2$, (c) TiSeO/MoSe$_2$, and (d) TiSO/MoS$_2$.

$$\eta = \frac{(V_{oc}J_{sc}FF)}{P_{sun}}, \tag{3}$$

where, the open circuit voltage is denoted by V_{oc} (mV), J_{sc} (mA cm^{-2}) represent short circuit-current, FF is the fill factor and the total incident solar radiation is denoted by P_{solar} (W m^{-2}).

$$eV_{oc} = E_g - E_{loss}, \tag{4}$$

where, E_g is band gap, J_{sc} denotes the maximum short-circuit current density and calculated as shown, and $S(E)$ is calculated using the NREL AM1.5 dataset.

$$J_{sc} = e \int_{E_g}^{\infty} \frac{SE}{E} d(E), \tag{5}$$

P_{sun} is calculated using eqn (5):

$$P_{sun} = \int_{0}^{\infty} S(E)d(E), \tag{6}$$

In 2D heterostructure solar cell structures, fill factors are commonly in the 0.3–0.5 range,[66] so we considered this value. We use a value of 0.3 for energy loss (E_{loss}).[66,67]

The PCE values that were computed are shown in Table 2 above. The calculated PCE with respect to band gap can be divided in to two groups: the optimum PCE, of which five of the materials are nearly in the optimal range, obtained at a band gap of $1 < E_g < 1.45$ eV, which is between 10 to 18 percent for a fill factor 3 to 5 respectively. As a result, we conclude that MXO/MoX$_2$ heterostructure material with direct band gap values it is suitable for photovoltaic cell1 with a very good efficiency. The PCE for the structures which have a band gap of $E_g < 1$ eV & $E_g >$ 1.45 eV are between 5–10% and 7–15% respectively. Because the PBE functional underestimates the band gap, we used the hybrid density functional Heyd–Scuseria–Ernzerhof (HSE06) to obtain more accurate results. Table S3, Fig. S7 and S8† provide additional information on the obtained results. In terms of PCE, the material studied, it is significantly superior than the following heterostructure materials FF 0.57 MoS$_2$/WSSe (9.37%),[11] with fill factor of 0.31 WSe$_2$/MoS$_2$ (4.32%),[68] for FF 57% MoS$_2$/P-Si (5.23%).[69]

Table 2 Shows the calculated efficiency of photovoltaic conversion

Janus/TMDs	Band gap (eV) HSE06	Band gap (eV) PBE	PCE (%)
H-HfSeO/MoSe$_2$	1.655	1.396	10.68–17.80
H-TiSeO/MoSe$_2$	2.202	1.443	10.45–17.42
H-HfSO/MoS$_2$	2.102	1.669	9.26–15.43
H-TiSO/MoS$_2$	2.701	1.972	7.17–11.95
T-HfSeO/MoSe$_2$	0.714	0.525	4.57–7.61
T-TiSeO/MoSe$_2$	1.303	1.014	10.19–16.98
T-HfSO/MoS$_2$	1.205	1.056	10.30–17.17
T-TiSO/MoS$_2$	1.824	1.464	10.34–17.23

4 Conclusion

The structural, electrical, and optical properties of MXO/MoX$_2$ hexagonal and distorted heterostructure materials were investigated. All of these compounds are semiconductors. MXO/MoX$_2$ semiconductors absorb more visible light and gather photons more efficiently from visible to ultraviolet wavelengths. This implies that these materials have a high solar energy absorption efficiency and, as a result, a higher photovoltaic efficiency. This provides the best opportunity to create new materials. It should be mentioned that the two basic criteria for solar cell materials are: with a band gap ranging from 1.0 eV to 2.0 eV and having a high optical absorption. The photovoltaic activities of the hetero structure are superior due to the very effective charge separation caused by the direct band nature, as well as the high optical absorption coefficient in the visible area. The calculated Power conversion efficiency values computed indicate best efficient solar cells for next-generation energy harvesting applications. As a result, it was observed that MXO/MoX$_2$ vdW heterostructures were discovered to have excellent electrical and optical properties, as well as a high photovoltaic conversion efficiency, making them attractive for use in solar cells.

Conflicts of interest

There are no conflicts to declare.

Acknowledgements

References

1 T. l. Bahers, M. Rérat and P. Sautet, Semiconductors Used in Photovoltaic and Photocatalytic Devices: Assessing Fundamental Properties from DFT, *J. Phys. Chem. C*, 2014, **118**(12), 5997–6008, DOI: **10.1021/jp409724c**.

2 M. R. Ashwin Kishore, K. Larsson and P. Ravindran, Two-Dimensional CdX/C$_2$N (X = S, Se) Heterostructures as Potential Photocatalysts for Water Splitting: A DFT Study, *ACS Omega*, 2020, **5**(37), 23762–23768, DOI: **10.1021/acsomega.0c02804**.

3 D. Gielen, F. Boshell, D. Saygin, M. D. Bazilian, N. Wagner and R. Gorini, The Role of Renewable Energy in the Global Energy Transformation, *Energy Strategy Reviews*, 2019, **24**, 38–50, DOI: **10.1016/j.esr.2019.01.006**.

4 T. Su, Q. Shao, Z. Qin, Z. Guo and Z. Wu, Role of Interfaces in Two-Dimensional Photocatalyst for Water Splitting, *ACS Catal.*, 2018, **8**(3), 2253–2276, DOI: **10.1021/acscatal.7b03437**.

5 J. A. Luceño-Sánchez, A. M. Díez-Pascual and R. P. Capilla, Materials for Photovoltaics: State of Art and Recent Developments, *Int. J. Mol. Sci.*, 2019, **20**(4), 976, DOI: **10.3390/ijms20040976**.

6 L. Seixas, Janus Two-Dimensional Materials Based on Group IV Monochalcogenides, *J. Appl. Phys.*, 2020, **128**, 045115, DOI: **10.1063/5.0012427**.

7 O. A. Al-Shahri, F. B. Ismail, M. A. Hannan, M. S. H. Lipu, A. Q. Al-Shetwi, R. A. Begum, N. F. O. Al-Muhsen and E. Soujeri, Solar Photovoltaic Energy Optimization Methods, Challenges and Issues: A Comprehensive Review, *J. Cleaner Prod.*, 2021, **284**, 125465, DOI: **10.1016/j.jclepro.2020.125465**.

8 A. A. F. Husain, W. Z. W. Hasan, S. Shafie, M. N. Hamidon and S. S. Pandey, A Review of Transparent Solar Photovoltaic Technologies, *Renewable Sustainable Energy Rev.*, 2018, 779–791, DOI: **10.1016/j.rser.2018.06.031**.

9 Y. L. Liu, Y. Shi and C. L. Yang, Two-Dimensional MoSSe/g-GeC van Der Waals Heterostructure as Promising Multifunctional System for Solar Energy Conversion, *Appl. Surf. Sci.*, 2021, **545**, 148952, DOI: **10.1016/j.apsusc.2021.148952**.

10 X. H. Li, B. J. Wang, H. Li, X. F. Yang, R. Q. Zhao, X. T. Jia and S. H. Ke, Two-Dimensional Layered Janus-In$_2$SeTe/C$_2$N van Der Waals Heterostructures for Photocatalysis and Photovoltaics: First-Principles Calculations, *New J. Chem.*, 2020, **44**(37), 16092–16100, DOI: **10.1039/d0nj03296d**.

11 B. T. Beshir, K. O. Obodo and G. A. Asres, Janus Transition Metal Dichalcogenides in Combination with MoS$_2$ for High-Efficiency Photovoltaic Applications: A DFT Study, *RSC Adv.*, 2022, **12**(22), 13749–13755, DOI: **10.1039/d2ra00775d**.

12 B. Peng, P. K. Ang and K. P. Loh, Two-Dimensional Dichalcogenides for Light-Harvesting Applications, *Nano Today*, 2015, 128–137, DOI: **10.1016/j.nantod.2015.01.007**.

13 A. O. M. Almayyali, B. B. Kadhim and H. R. Jappor, Stacking Impact on the Optical and Electronic Properties of Two-Dimensional MoSe$_2$/PtS$_2$ Heterostructures Formed by PtS$_2$ and MoSe$_2$ Monolayers, *Chem. Phys.*, 2020, **532**, 110679, DOI: **10.1016/j.chemphys.2020.110679**.

14 Y. Yan, Z. Zeng, M. Huang and P. Chen, Van Der Waals Heterojunctions for Catalysis, *Mater. Today Adv.*, 2020, **6**, 100059, DOI: **10.1016/j.mtadv.2020.100059**.

15 K. Rahimi, Electric-Field- and Strain-Induced Adjustability of VdW Heterostructure of g-ZnO/2H-TiS$_2$ for Optoelectronic Applications, *Mater. Lett.*, 2021, **282**, 128680, DOI: **10.1016/j.matlet.2020.128680**.

16 Q. Alam, M. Idrees, S. Muhammad, C. v. Nguyen, M. Shafiq, Y. Saeed, H. U. Din and B. Amin, Stacking Effects in van der Waals Heterostructures of BlueP and Janus XYO (X = Ti, Zr, Hf: Y = S, Se) Monolayers, *RSC Adv.*, 2021, **11**(20), 12189–12199, DOI: **10.1039/d0ra10827h**.

17 Q. Alam, M. Idrees, S. Muhammad, C. v. Nguyen, M. Shafiq, Y. Saeed, H. U. Din and B. Amin, Stacking Effects in van der Waals Heterostructures of BlueP and Janus XYO (X = Ti, Zr, Hf: Y = S, Se) Monolayers, *RSC Adv.*, 2021, **11**(20), 12189–12199, DOI: **10.1039/d0ra10827h**.

18 M. Yagmurcukardes, Y. Qin, S. Ozen, M. Sayyad, F. M. Peeters, S. Tongay and H. Sahin, Quantum Properties and Applications of 2D Janus Crystals and Their Superlattices, *Appl. Phys. Rev.*, 2020, **7**, 011311, DOI: **10.1063/1.5135306**.

19 C. H. Yeh, Computational Study of Janus Transition Metal Dichalcogenide Monolayers for Acetone Gas Sensing, *ACS Omega*, 2020, **5**(48), 31398–31406, DOI: **10.1021/acsomega.0c04938**.

20 M. Mohl, A. R. Rautio, G. A. Asres, M. Wasala, P. D. Patil, S. Talapatra and K. Kordas, 2D Tungsten Chalcogenides: Synthesis, Properties and Applications, *Adv. Mater. Interfaces*, 2020, **7**, 2000002, DOI: **10.1002/admi.202000002**.

21 R. Li, Y. Cheng and W. Huang, Recent Progress of Janus 2D Transition Metal Chalcogenides: From Theory to Experiments, *Small*, 2018, **14**, 1802091, DOI: **10.1002/smll.201802091**.

22 A. Rawat, M. K. Mohanta, N. Jena, Dimple, R. Ahammed and A. de Sarkar, Nanoscale Interfaces of Janus Monolayers of Transition Metal Dichalcogenides for 2D Photovoltaic and Piezoelectric Applications, *J. Phys. Chem. C*, 2020, **124**(19), 10385–10397, DOI: **10.1021/acs.jpcc.0c02199**.

23 L. Zhang, Z. Yang, T. Gong, R. Pan, H. Wang, Z. Guo, H. Zhang and X. Fu, Recent Advances in Emerging Janus Two-Dimensional Materials: From Fundamental Physics to Device Applications, *J. Mater. Chem. A*, 2020, **8**, 8813–8830, DOI: **10.1039/d0ta01999b**.

24 X. Zhang, X. Yuan, L. Jiang, J. Zhang, H. Yu, H. Wang and G. Zeng, Powerful Combination of 2D g-C$_3$N$_4$ and 2D Nanomaterials for Photocatalysis: Recent Advances, *Chem. Eng. J.*, 2020, **390**, 124475, DOI: **10.1016/j.cej.2020.124475**.

25 A. C. Riis-Jensen, T. Deilmann, T. Olsen and K. S. Thygesen, Classifying the Electronic and Optical Properties of Janus Monolayers, *ACS Nano*, 2019, **13**(11), 13354–13364, DOI: **10.1021/acsnano.9b06698**.

26 H. Ye, H. Sheng, D. Bai, J. Zhang and J. Wang, Strain and Electric Field Tuned Electronic Properties of BAs/MoSe$_2$ van der Waals Heterostructures for Alternative Electrodes and Photovoltaic Cell in Photocatalysis, *Phys. E*, 2020, **120**, 114055, DOI: **10.1016/j.physe.2020.114055**.

27 S. Bellani, A. Bartolotta, A. Agresti, G. Calogero, G. Grancini, A. di Carlo, E. Kymakis and F. Bonaccorso, Solution-Processed Two-Dimensional Materials for next-Generation Photovoltaics, *Chem. Soc. Rev.*, 2021, 11870–11965, DOI: **10.1039/d1cs00106j**.

28 S. Wang, C. Ren, H. Tian, J. Yu and M. Sun, MoS$_2$/ZnO van der Waals Heterostructure as a High-Efficiency Water Splitting Photocatalyst: A First-Principles Study, *Phys. Chem. Chem. Phys.*, 2018, **20**(19), 13394–13399, DOI: **10.1039/c8cp00808f**.

29 M. Cao, L. Ni, Z. Wang, J. Liu, Y. Tian, Y. Zhang, X. Wei, T. Guo, J. Fan and L. Duan, DFT Investigation on Direct Z-

Scheme Photocatalyst for Overall Water Splitting: MoTe₂/BAs van der Waals Heterostructure, *Appl. Surf. Sci.*, 2021, **551**, 149364, DOI: 10.1016/j.apsusc.2021.149364.

30 R. Michal, S. Sfaelou and P. Lianos, Photocatalysis for Renewable Energy Production Using Photofuelcells, *Molecules*, 2014, **19**(12), 19732–19750, DOI: 10.3390/molecules191219732.

31 M. B. Tahir, N. Fatima, U. Fatima and M. Sagir, A Review on the 2D Black Phosphorus Materials for Energy Applications, *Inorg. Chem. Commun.*, 2021, **124**, 108242, DOI: 10.1016/j.inoche.2020.108242.

32 R. Tong, K. W. Ng, X. Wang, S. Wang, X. Wang and H. Pan, Two-Dimensional Materials as Novel Co-Catalysts for Efficient Solar-Driven Hydrogen Production, *J. Mater. Chem. A*, 2020, 23202–23230, DOI: 10.1039/d0ta08045d.

33 A. C. Riis-Jensen, M. Pandey and K. S. Thygesen, Efficient Charge Separation in 2D Janus van der Waals Structures with Built-in Electric Fields and Intrinsic p–n Doping, *J. Phys. Chem. C*, 2018, **122**(43), 24520–24526, DOI: 10.1021/acs.jpcc.8b05792.

34 L. Ju, M. Bie, X. Zhang, X. Chen and L. Kou, Two-Dimensional Janus van der Waals Heterojunctions: A Review of Recent Research Progresses, *Front. Phys.*, 2021, **16**(1), 13201, DOI: 10.1007/s11467-020-1002-4.

35 K. Ren, M. L. Sun, Y. Luo, S. K. Wang, J. Yu and W. C. Tang, First-Principle Study of Electronic and Optical Properties of Two-Dimensional Materials-Based Heterostructures Based on Transition Metal Dichalcogenides and Boron Phosphide, *Appl. Surf. Sci.*, 2019, **476**, 70–75, DOI: 10.1016/j.apsusc.2019.01.005.

36 X. Liu, P. Gao, W. Hu and J. Yang, Photogenerated-Carrier Separation and Transfer in Two-Dimensional Janus Transition Metal Dichalcogenides and Graphene van der Waals Sandwich Heterojunction Photovoltaic Cells, *J. Phys. Chem. Lett.*, 2020, **11**(10), 4070–4079, DOI: 10.1021/acs.jpclett.0c00706.

37 I. Shahid, A. Ali, J. M. Zhang, I. Muhammad, I. Ahmad and F. Kabir, Two Dimensional MoSSe/BSe VdW Heterostructures as Potential Photocatalysts for Water Splitting with High Carrier Mobilities, *Int. J. Hydrogen Energy*, 2021, **46**(27), 14247–14258, DOI: 10.1016/j.ijhydene.2021.01.157.

38 Z. Guan, C. S. Lian, S. Hu, S. Ni, J. Li and W. Duan, Tunable Structural, Electronic, and Optical Properties of Layered Two-Dimensional C₂N and MoS₂ van der Waals Heterostructure as Photovoltaic Material, *J. Phys. Chem. C*, 2017, **121**(6), 3654–3660, DOI: 10.1021/acs.jpcc.6b12681.

39 P. Giannozzi, O. Andreussi, T. Brumme, O. Bunau, M. Buongiorno Nardelli, M. Calandra, R. Car, C. Cavazzoni, D. Ceresoli, M. Cococcioni, N. Colonna, I. Carnimeo, A. Dal Corso, S. de Gironcoli, P. Delugas, R. A. Distasio, A. Ferretti, A. Floris, G. Fratesi, G. Fugallo, R. Gebauer, U. Gerstmann, F. Giustino, T. Gorni, J. Jia, M. Kawamura, H. Y. Ko, A. Kokalj, E. Kücükbenli, M. Lazzeri, M. Marsili, N. Marzari, F. Mauri, N. L. Nguyen, H. v. Nguyen, A. Otero-De-La-Roza, L. Paulatto, S. Poncé, D. Rocca, R. Sabatini, B. Santra, M. Schlipf,

A. P. Seitsonen, A. Smogunov, I. Timrov, T. Thonhauser, P. Umari, N. Vast, X. Wu and S. Baroni, Advanced Capabilities for Materials Modelling with Quantum ESPRESSO, *J. Phys.: Condens. Matter*, 2017, **29**, 465901, DOI: 10.1088/1361-648X/aa8f79.

40 R. Peng, Y. Ma, B. Huang and Y. Dai, Two-Dimensional Janus PtSSe for Photocatalytic Water Splitting under the Visible or Infrared Light, *J. Mater. Chem. A*, 2019, **7**(2), 603–610, DOI: 10.1039/c8ta09177c.

41 C. Nguyen, N. v. Hoang, H. v. Phuc, A. Y. Sin and C. v. Nguyen, Two-Dimensional Boron Phosphide/MoGe₂N₄ van der Waals Heterostructure: A Promising Tunable Optoelectronic Material, *J. Phys. Chem. Lett.*, 2021, **12**, 5076–5084, DOI: 10.1021/acs.jpclett.1c01284.

42 X. Wang, Y. Wang, R. Quhe, Y. Tang, X. Dai and W. Tang, Designing Strained C₂N/GaTe(InTe) Heterostructures for Photovoltaic and Photocatalytic Application, *J. Alloys Compd.*, 2020, **816**, 152559, DOI: 10.1016/j.jallcom.2019.152559.

43 M. Gajdoš, K. Hummer, G. Kresse, J. Furthmüller and F. Bechstedt, Linear Optical Properties in the Projector-Augmented Wave Methodology, *Phys. Rev. B: Condens. Matter Mater. Phys.*, 2006, **73**, 045112, DOI: 10.1103/PhysRevB.73.045112.

44 D. Jana, C. L. Sun, L. C. Chen and K. H. Chen, Effect of Chemical Doping of Boron and Nitrogen on the Electronic, Optical, and Electrochemical Properties of Carbon Nanotubes, *Prog. Mater. Sci.*, 2013, **58**, 565–635, DOI: 10.1016/j.pmatsci.2013.01.003.

45 S. Brodersen, D. Lukas and W. Schattke, Calculation of the Dielectric Function in a Local Representation, *Phys. Rev. B: Condens. Matter Mater. Phys.*, 2002, **66**, 085111, DOI: 10.1103/PhysRevB.66.085111.

46 N. Wiser, Dielectric Constant with Local Field Effects Included, *Phys. Rev.*, 1963, **129**, 62–69, DOI: 10.1103/PhysRev.129.62.

47 Z. Haman, M. Kibbou, I. Bouziani, Y. Benhouria, I. Essaoudi, A. Ainane and R. Ahuja, Structural, Electronic and Optical Properties of Two-Dimensional Janus Transition Metal Oxides MXO (M = Ti, Hf and Zr; X = S and Se) for Photovoltaic and Opto-Electronic Applications, *Phys. B*, 2021, **604**, 412621, DOI: 10.1016/j.physb.2020.412621.

48 Q. Li, L. Xu, K. W. Luo, L. L. Wang and X. F. Li, SiC/MoS₂ Layered Heterostructures: Promising Photocatalysts Revealed by a First-Principles Study, *Mater. Chem. Phys.*, 2018, **216**, 64–71, DOI: 10.1016/j.matchemphys.2018.05.063.

49 T. Teshome and A. Datta, Two-Dimensional Graphene–Gold Interfaces Serve as Robust Templates for Dielectric Capacitors, *ACS Appl. Mater. Interfaces*, 2017, **9**(39), 34213–34220, DOI: 10.1021/acsami.7b09360.

50 P. T. T. Le, L. M. Bui, N. N. Hieu, H. v. Phuc, B. Amin, N. v. Hieu and C. v. Nguyen, Tailoring Electronic Properties and Schottky Barrier in Sandwich Heterostructure Based on Graphene and Tungsten Diselenide, *Diamond Relat. Mater.*, 2019, **94**, 129–136, DOI: 10.1016/j.diamond.2019.02.025.

51 A. A. Attia and H. R. Jappor, Tunable Electronic and Optical Properties of New Two-Dimensional GaN/BAs van der Waals Heterostructures with the Potential for Photovoltaic Applications, *Chem. Phys. Lett.*, 2019, **728**, 124–131, DOI: **10.1016/j.cplett.2019.05.005**.

52 W. Hu, T. Wang, R. Zhang and J. Yang, Effects of Interlayer Coupling and Electric Fields on the Electronic Structures of Graphene and MoS_2 Heterobilayers, *J. Mater. Chem. C*, 2016, **4**(9), 1776–1781, DOI: **10.1039/c6tc00207b**.

53 D. L. Duong, S. J. Yun and Y. H. Lee, van der Waals Layered Materials: Opportunities and Challenges, *ACS Nano*, 2017, 11803–11830, DOI: **10.1021/acsnano.7b07436**.

54 M. M. Obeid, A. Bafekry, S. Ur Rehman and C. v. Nguyen, A Type-II $GaSe/HfS_2$ van der Waals Heterostructure as Promising Photocatalyst with High Carrier Mobility, *Appl. Surf. Sci.*, 2020, **534**, 147607, DOI: **10.1016/j.apsusc.2020.147607**.

55 C. Li, Q. Cao, F. Wang, Y. Xiao, Y. Li, J. J. Delaunay and H. Zhu, Engineering Graphene and TMDs Based van der Waals Heterostructures for Photovoltaic and Photoelectrochemical Solar Energy Conversion, *Chem. Soc. Rev.*, 2018, 4981–5037, DOI: **10.1039/c8cs00067k**.

56 H. Zheng, X. b. Li, N. K. Chen, S. Y. Xie, W. Q. Tian, Y. Chen, H. Xia, S. B. Zhang and H. B. Sun, Monolayer II-VI Semiconductors: A First-Principles Prediction, *Phys. Rev. B: Condens. Matter Mater. Phys.*, 2015, **92**, 115307, DOI: **10.1103/PhysRevB.92.115307**.

57 A. A. Attia and H. R. Jappor, Tunable Electronic and Optical Properties of New Two-Dimensional GaN/BAs van der Waals Heterostructures with the Potential for Photovoltaic Applications, *Chem. Phys. Lett.*, 2019, **728**, 124–131, DOI: **10.1016/j.cplett.2019.05.005**.

58 I. Allaoui, A. Benyoussef and A. el Kenz, Two-Dimensional SnTe/Sb van der Waals Heterostructure for Photovoltaic Application, *Solid State Sci.*, 2021, **121**, 106736, DOI: **10.1016/j.solidstatesciences.2021.106736**.

59 J. R. Zhang, Y. Q. Zhao, L. Chen, S. F. Yin and M. Q. Cai, Density Functional Theory Calculation on Facet-Dependent Photocatalytic Activity of MoS_2/CdS Heterostructures, *Appl. Surf. Sci.*, 2019, **469**, 27–33, DOI: **10.1016/j.apsusc.2018.11.004**.

60 C. Boix-Constant, S. Mañas-Valero, R. Córdoba and E. Coronado, Van Der Waals Heterostructures Based on Atomically-Thin Superconductors, *Adv. Electron. Mater.*, 2021, **7**(7), 2000987, DOI: **10.1002/aelm.202000987**.

61 A. Rai, H. C. P. Movva, A. Roy, D. Taneja, S. Chowdhury and S. K. Banerjee, Progress in Contact, Doping and Mobility Engineering of MoS_2: An Atomically Thin 2D Semiconductor, *Crystals*, 2018, **8**(8), 316, DOI: **10.3390/cryst8080316**.

62 M. Kumar, A. Raj, A. Kumar and A. Anshul, Effect of Band-Gap Tuning on Lead-Free Double Perovskite Heterostructure Devices for Photovoltaic Applications via SCAPS Simulation, *Mater. Today Commun.*, 2021, **26**, 101851, DOI: **10.1016/j.mtcomm.2020.101851**.

63 J. Kusuma, R. Geetha Balakrishna and B. D. C. O. E. Sewagram, A review on electrical characterization techniques performed to study the device performance of quantum dot sensitized solar cells, *Sol. Energy*, 2018, **159**, 682–696.

64 P. K. Nayak, S. Mahesh, H. J. Snaith and D. Cahen, Photovoltaic Solar Cell Technologies: Analysing the State of the Art, *Nat. Rev. Mater.*, 2019, **4**(4), 269–285, DOI: **10.1038/s41578-019-0097-0**.

65 M. R. Filip, C. Verdi and F. Giustino, GW Band Structures and Carrier Effective Masses of $CH_3NH_3PbI_3$ and Hypothetical Perovskites of the Type $APbI_3$: A = NH_4, PH_4, AsH_4, and SbH_4, *J. Phys. Chem. C*, 2015, **119**(45), 25209–25219, DOI: **10.1021/acs.jpcc.5b07891**.

66 M. M. Furchi, F. Höller, L. Dobusch, D. K. Polyushkin, S. Schuler and T. Mueller, Device Physics of van der Waals Heterojunction Solar Cells, *npj 2D Mater. Appl.*, 2018, **2**, 3, DOI: **10.1038/s41699-018-0049-3**.

67 K. Lai, C. L. Yan, L. Q. Gao and W. B. Zhang, AI_3 (A = As, Sb) Single Layers and Their VdW Heterostructure for Photocatalysis and Solar Cell Applications, *J. Phys. Chem. C*, 2018, **122**(14), 7656–7663, DOI: **10.1021/acs.jpcc.8b01874**.

68 A. J. Cho, M. K. Song, D. W. Kang and J. Y. Kwon, Two-Dimensional WSe_2/MoS_2 p–n Heterojunction-Based Transparent Photovoltaic Cell and Its Performance Enhancement by Fluoropolymer Passivation, *ACS Appl. Mater. Interfaces*, 2018, **10**, 35972–35977, DOI: **10.1021/acsami.8b12250**.

69 M. L. Tsai, S. H. Su, J. K. Chang, D. S. Tsai, C. H. Chen, C. I. Wu, L. J. Li, L. J. Chen and J. H. He, Monolayer MoS_2 Heterojunction Solar Cells, *ACS Nano*, 2014, **8**(8), 8317–8322, DOI: **10.1021/nn502776h**.